Structural Diversity of Rare-Earth Oxychalcogenides

Melissa Orr, Glen R. Hebberd, Emma E. McCabe, and Robin T. Macaluso*

Read Online

ACCESS | Metrics & More | Article Recommendations | Supporting Information

ABSTRACT: Mixed-anion systems have garnered much attention in the past decade with attractive properties for diverse applications such as energy conversion, electronics, and catalysis. The discovery of new materials through mixed-cation and single-anion systems proved highly successful in the previous century, but solid-state chemists are now embracing an exciting design opportunity by incorporating multiple anions in compounds such as oxychalcogenides. Materials containing rare-earth ions are arguably a cornerstone of modern technology, and herein, we review recent advances in rare-earth oxychalcogenides. We discuss ternary rare-earth oxychalcogenides whose layered structures illustrate the characters and bonding preferences of oxide and chalcogenide anions. We then review quaternary compounds which combine anionic and cationic design strategies toward materials discovery and describe their structural diversity. Finally, we emphasize the progression from layered two-dimensional compounds to three-dimensional networks and the unique synthetic approaches which enable this advancement.
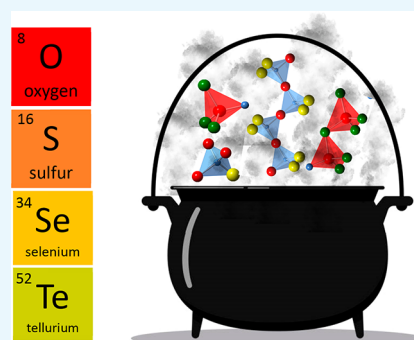
INTRODUCTION

The design and synthesis of new functional materials has long been dominated by work on single-anion compounds such as metal oxides, chalcogenides, and pnictides where cation composition is used to tune properties.[1] Mixed-anion systems, on the other hand, are comparatively underexplored. Mixed-anion systems contain multiple negatively charged anions, such as oxysulfides, with both oxide (O^{2-}) and sulfide (S^{2-}) ions. These are distinct from materials containing polyatomic anions such as sulfate (SO_4^{2-}) or sulfite (SO_3^{2-}) anions, in which the sulfur species has a positive formal oxidation state (+6 and +4 in sulfate and sulfite ions, respectively).

Rare-earth oxychalcogenides have been of interest since the implementation of Ln_2O_2S as phosphors for cathode ray tubes in the middle of the twentieth century. The recent resurgence of interest in oxychalcogenides is perhaps a result of modern computationally driven materials screening techniques, for which several recent publications point out the promise of oxychalcogenides in various applications, such as p-type transparent semiconductors,[2,3] thermoelectrics,[4,5] and solid-state electrolytes.[6] Advancements in synthetic strategies to control chemical and physical properties by mixing anions has been recently reviewed.[7,8]

Oxychalcogenides, containing O^{2-} and Q^{2-} (where Q = S, Se, or Te), are *rarely* simply anion-substituted analogues of the single-anion oxide or chalcogenide materials. The diverse relationships between the structures of mixed-anion compounds and structures of single-anion compounds were first pointed out 70 years ago.[9] Many mixed-anion materials adopt distinct structure types, local coordination environments, and dimensionality.[10]

Herein, we discuss critical structural features of oxychalcogenides. We emphasize that understanding the crystal structures of oxychalcogenides with an appreciation of chemical concepts, e.g., ionic radii, electronegativity, and polarizability, and hard−soft acid base theory, will lead toward a better grasp of synthetic challenges and a better rationalization of their electronic structures and physical behavior. The number of metal oxychalcogenides is huge, so we use this mini-review to focus on ternary rare-earth oxychalcogenides as a foundation for identifying key structural building blocks that, if exploited creatively, will advance materials discovery of oxychalcogenide materials. We then progress toward a discussion on recent discoveries of quaternary rare-earth oxychalcogenides that expand our understanding of crystal structures of mixed-anion materials. Rare-earth oxychalcogenides present an opportunity to combine metals of varying hardness (or softness) that yield new structures and interesting physical properties, e.g., magnetism and photoluminescence. The focus of this mini-review is the developments of rare-earth oxychalcogenides over the past ∼10 years. Information on this topic prior to the last 10 years can be found in references 10−13.
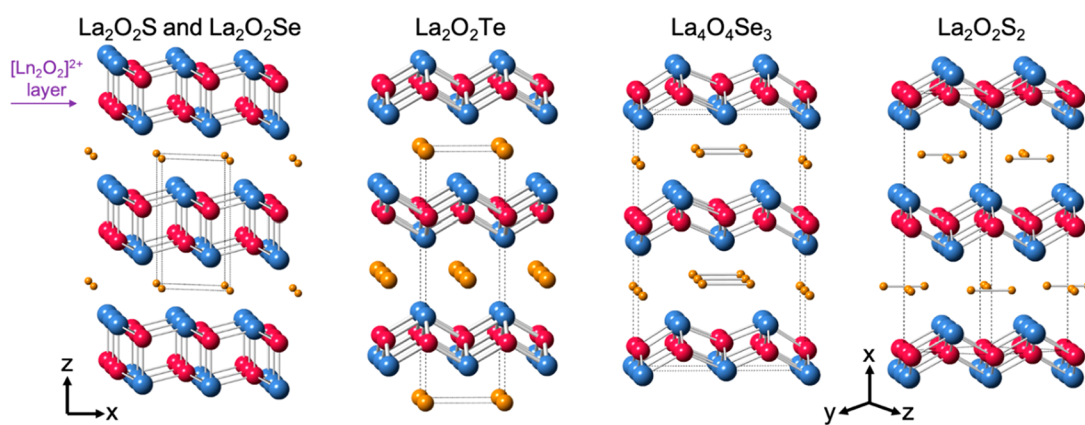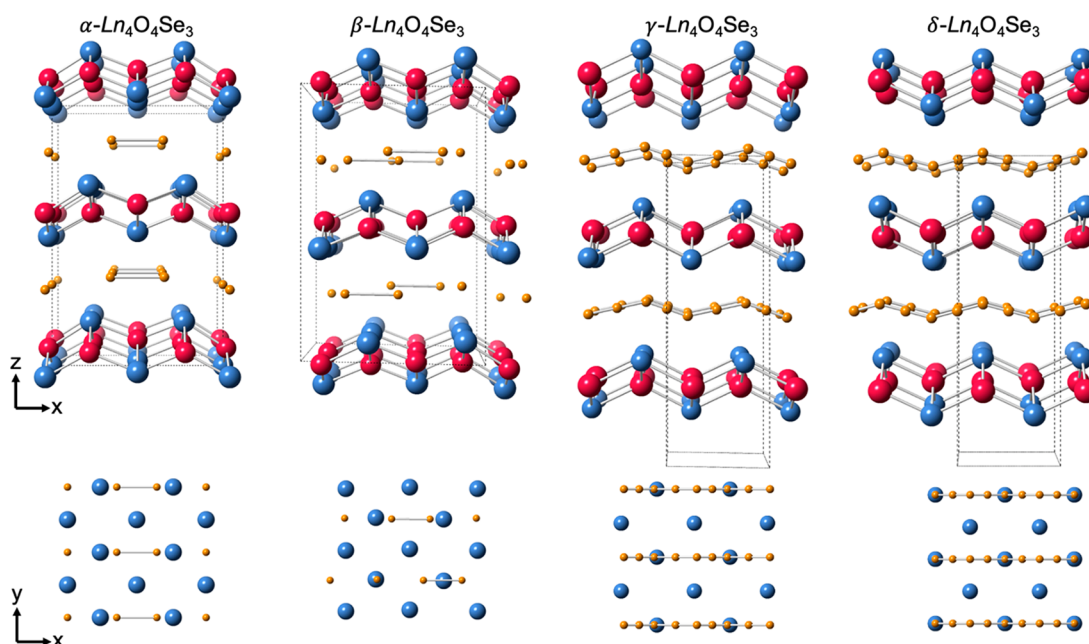
Figure 1. Structure types of $La_2O_2S(Se)$, anti-$ThCr_2Si_2$ (La_2O_2Te), $La_4O_4Q_3$, and $La_2O_2S_2$, with La, O, and Q ions shown in blue, pink, and yellow, respectively. The fundamental $[Ln_2O_2]^{2+}$ layer consists of edge-linked OLn_4 tetrahedra.

Figure 2. Polymorph structures of $Ln_4O_4Se_3$, with Ln, O, and Se ions shown in blue, pink, and yellow, respectively. View of Ln and Q relation along [001] shown below each polymorph structure.
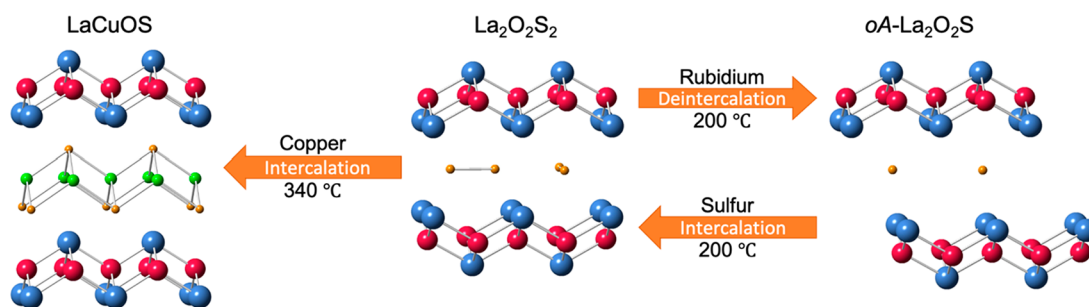
TERNARY OXYCHALCOGENIDES

Ternary rare-earth oxychalcogenides can be found in a variety of compositional ratios. Most oxygen-rich materials reported from conventional solid-state routes belong to four structure types: La_2O_2S (including La_2O_2Se), anti-$ThCr_2Si_2$ (La_2O_2Te), $La_4O_4Se_3$, and $La_2O_2S_2$.[14−16] These structures, illustrated in Figure 1, provide an excellent starting point from which to explore the structural chemistry and physical properties of oxychalcogenides. In all four structure types, oxygen and chalcogen species are separated into two distinct layers—one layer of edge-sharing $[Ln_2O_2]^{2+}$ units and one chalcogenide layer. This separation of anions is not surprising given the relative softness of S, Se, and Te compared to that of O.

$[Ln_2O_2]^{2+}$ **Layer in Ternary Oxychalcogenides.** The OLn_4 building unit (O-centered tetrahedron, Ln = lanthanide cation) is a common structural feature in oxychalcogenides. Two-dimensional $[Ln_2O_2]^{2+}$ layers composed of fluorite-like edge-linked OLn_4 tetrahedra are quite robust; they are observed in all four structures with only slight distortions or variations in their symmetry with respect to the next $[Ln_2O_2]^{2+}$ layer. For example, OLn_4 units form trigonal $[Ln_2O_2]^{2+}$ layers which are simply translated along the c-axis in La_2O_2S, whereas the tetragonal $[Ln_2O_2]^{2+}$ layers are related by an ab-mirror plane in La_2O_2Te and by a glide plane in $La_4O_4Se_3$. Replacing Ln^{3+} with Bi^{3+} gives the closely related Bi_2O_2Q (Q = S, Se, Te) series, with the oxyselenide and oxytelluride isostructural with La_2O_2Te (Figure 1),[5,17] whereas the oxysulfide Bi_2O_2S adopts a similar structure with a slight orthorhombic distortion.[18] Interestingly, the relative softness of the Bi^{3+} cation also allows it to occupy sites occupied by softer Q, leading to Bi−O−Q phases containing both $[Bi_2O_2]^{2+}$ and Bi−Q layers and giving structures more akin to those adopted by quaternary systems (see below).[19]

CHALCOGENIDE LAYERS IN TERNARY OXYCHALCOGENIDES

Monoatomic Anion Only. It is the chalcogen layer that exhibits the greater structural diversity. Within these ternary materials, the chalcogen species can be found as $Q^{2−}$ ions and $(Q_2)^{2−}$ dimers. In La_2O_2S and anti-$ThCr_2Si_2$ (La_2O_2Te)

Figure 3. Topochemical reactions of $La_2O_2S_2$ yield oA-La_2O_2S and LaCuOS, with La, Cu, O, and S ions shown in blue, green, pink, and yellow, respectively.
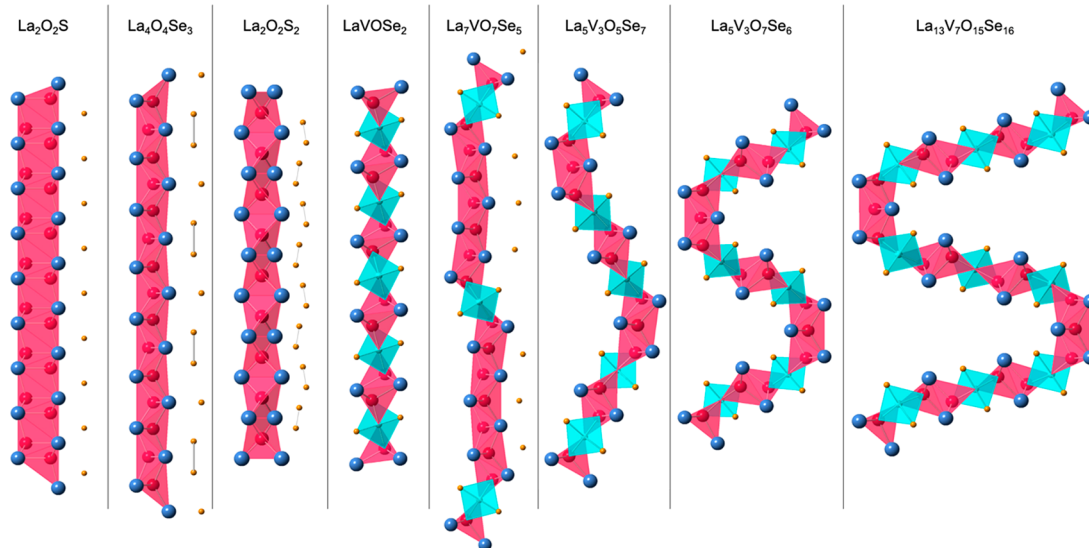
Figure 4. Structural units composed of tetrahedral OLa_4 units among ternary oxychalcogenides and quaternary rare-earth vanadium oxyselenides, with La, V, O and Se ions shown in blue, cyan, pink, and yellow, respectively.

structure types, the chalcogen species occur as chalcogenide Q^{2-} ions and are separated from each other by ~4 Å in the $[Ln_2O_2]^{2+}$ layers.

The expected oxidation state of S^{2-} in Ln_2O_2S compounds can deviate by including mixed-valent $Ce^{3+/4+}$. Upon exposure to air, S^{2-} can also be oxidized to S^{4+} and S^{6+} species in $Gd_{2(1-y)}Ce_{2y}O_2S$ nanoparticles.[20] This helps to illustrate the instability of many oxychalcogenides.

Monoatomic Anion and Dimers. α-$La_4O_4Se_3$ contains both chalcogenide Se^{2-} ions as well as Se species separated by only ~2.45 Å;[15] this falls within the 2.3−2.5 Å range observed for $(Se_2)^{2-}$ dimers in binary metal polyselenides.[21]

The structural chemistry of the chalcogen layers is not independent from that of the oxide layers. In the β-polymorph of the $La_4O_4Se_3$ structure adopted by $Eu_4O_4Se_3$, the staggered arrangement of $(Se_2)^{2-}$ and Se^{2-} ions, as shown in Figure 2, lowers the symmetry of the Eu sites with implications for its electronic structure.[22] Calculations of the partial density of states show that the Eu 4f, O 2p, and Se 4p orbitals dominate the valence band while the $(Se_2)^{2-}$ and Eu 5d orbitals make up the conduction band. The separation of the $(Se_2)^{2-}$ and Se^{2-} p-orbitals raises the question of how structural diversity within the chalcogenide layers influence semiconducting behavior. Increased complexity is observed in the γ and δ structures, formed by Ln = Gd, Tb and Ln = Dy, Ho, Er, Yb, Y, respectively. The Se layer in both forms has been described as

multiple chains of ordered $(Se_2)^{2-}$ and Se^{2-} that are arranged in a disordered zigzag wave of Se (Figure 2).

Dimers Only. Chalcogenide dimer units are also observed in $La_2O_2S_2$, whose chalcogen layer is composed solely of $(S_2)^{2-}$ dimers. These dimers have a bond length of ~2.1 Å, typical of S−S single bond.[23] The dimers in $La_2O_2S_2$ can be exploited by topochemical reactions to give new materials (Figure 3). Upon reaction of $La_2O_2S_2$ with Rb metal, the $(S_2)^{2-}$ dimers can be reduced, thereby deintercalating sulfur from the parent $La_2O_2S_2$ compound.[24] The product of the deintercalation, coined oA-La_2O_2S (where oA refers to the orthorhombic $Amm2$ space group), has a distinct structure from La_2O_2S discussed previously. In oA-La_2O_2S, every other $[La_2O_2]^{2+}$ layer is shifted along the $1/2(b + c)$ direction while the tetrahedral OLa_4 units themselves are maintained. The formation of oA-La_2O_2S cannot be achieved by high-temperature methods because it is a metastable product with a relative energy of 72 meV/atom higher than that of the ground-state La_2O_2S (prepared by high-temperature routes).

Sulfur can be (re)intercalated into the structure by heating oA-La_2O_2S with elemental sulfur. Partial deintercalation of the $(S_2)^{2-}$ dimers in $La_2O_2S_2$ leads to $La_2O_2S_{1.5}$, suggesting that topochemical routes may inspire the discovery of new oxychalcogenide phases.[24] Sulfur bonding proved to be a critical factor in optical behavior of the oxychalcogenides: the absorption edge (2.56 eV) arises from the $\pi^* \rightarrow \sigma^*$ electronic transition of sulfur pairs. Deintercalation of sulfur—removing
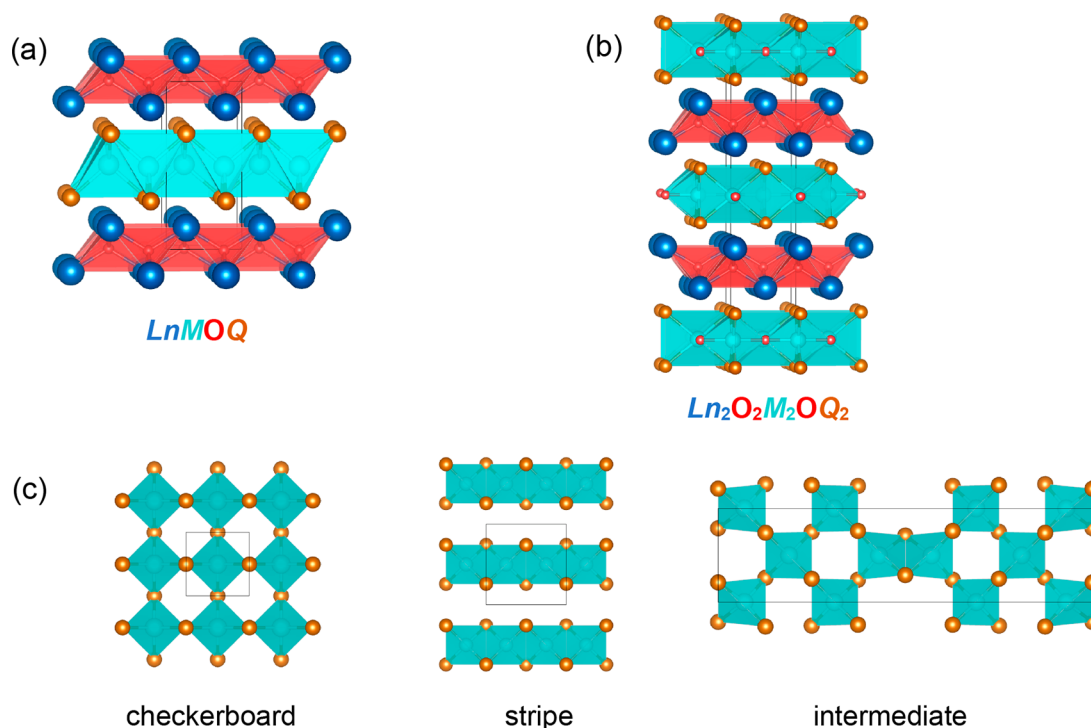
Figure 5. Quaternary Ln−M−O−Q oxychalcogenides with structures containing 2D $[Ln_2O_2]^{2+}$ layers including (a) ZrCuSiAs structure for LnMOQ phases, (b) $Ln_2O_2M_2OQ_2$ phases, and (c) MQ_2 layers (from above) in cation-ordered ZrCuSiAs-related phases $Ln_2O_2MQ_2$ containing M^{2+} ions, with Ln, M, O, and Q ions shown in blue, cyan, pink, and yellow, respectively.

the sulfur pairs—increases the absorption edge to 3.88 eV in oA-La$_2$O$_2$S. This is lower than the absorption onset of 4.13 eV observed for the thermodynamically stable hexagonal La$_2$O$_2$S, which arises from the S 3p → La 6s/5d transition associated with monatomic S^{2-} in La$_2$O$_2$S.[24]

QUATERNARY OXYCHALCOGENIDES

OLn$_4$ and OLn$_3$M Tetrahedra in Quaternary Oxychalcogenides. The ternary Ln−O−Q oxychalcogenides discussed above contain edge-linked OLn$_4$ tetrahedra to form 2D sheets, giving the layered crystal structures shown in Figure 1. The OLn$_4$ building unit (Ln = lanthanide or Bi^{3+} cation) is also common in quaternary lanthanide oxychalcogenides. The addition of a second metal M (M = transition metal or p block cation) in quaternary oxychalcogenides adds diversity to the packing of O-centered tetrahedral units. Depending on the hardness (or softness) of the second metal, the two-dimensional $[Ln_2O_2]^+$ sheet may be maintained, or discrete 2D $[Ln_2O_2]^{2+}$ fragments (consisting of only three or four OLn$_4$ units) or 1D ribbons of OLn$_4$ tetrahedral units may be observed instead. The connectivity of these OLn$_4$ units (and the possibility of including oxide ions in the coordination environment of the M^{x+} cation giving OLn$_3$M units) generates a huge diversity of structure types. This is perhaps best illustrated by the La−V−O−Se family of materials[25] (Figure 4) in which the OLn$_4$ units form 2D sheets of edge-connected tetrahedra as in La$_2$O$_2$S, 2D fragments (truncated by OLn$_3$V tetrahedra) as in La$_7$VO$_7$Se$_5$, and 1D ribbons of OLn$_4$ and OLn$_3$V tetrahedra as in La$_{13}$V$_7$O$_{15}$Se$_{16}$.

M−Q Bonding Motifs in Quaternary Oxychalcogenides. The relative softness of the M^{x+} cation (often a transition metal) compared to a rare-earth metal is appropriate for the introduction of M−Q bonding in quaternary oxychalcogenides. This can be understood in terms of allowing

ordering of the harder O^{2-} anions (coordinated predominantly by hard Ln^{3+} cations), whereas the softer S^{2-}/Se^{2-} anions are often coordinated by Ln^{3+} and the softer second cation M^{x+}.[26,27] The M−Q structures in these materials are very diverse, ranging from MQ$_4$ tetrahedra to MO$_x$Q$_{6-x}$ octahedra. The quaternary oxychalcogenides discussed in this mini-review are focused on M = transition metal; quaternary oxychalcogenides with M = p-block cation (e.g., Ga, Ge, As, In, Sn, Sb, Bi) exhibit interesting structures with separate O−Ln and M−Q sheets.[11,12]

Combined with the various structural motifs of OLn$_4$ units, the structures of quaternary oxychalcogenides become quite varied and complex. This categorization of quaternary lanthanide oxychalcogenides in terms of the connectivity of OLn$_4$ or OLn$_3$M units (2D sheets, 2D fragments, and 1D ribbons) is helpful to illustrate structural diversity as well as the factors that influence the structure(s) adopted by a given composition.

2D Sheets in Quaternary Oxychalcogenides. Continuous two-dimensional $[Ln_2O_2]^{2+}$ sheets of edge-shared OLn$_4$ tetrahedra as observed in ternary oxychalcogenides (Figures 1 and 2) are extended to quaternary oxychalcogenides including those of La$_2$O$_2$M$_2$OS$_2$,[28] ZrCuSiAs,[29] and cation-ordered ZrCuSiAs-related structural families. In these materials, $[Ln_2O_2]^{2+}$ sheets are separated by chalcogenide-rich layers (of net negative charge), and the layered structures of these materials (Figure 5) can have a significant role in determining physical properties.[30]

ZrCuSiAs structured materials are composed of alternating fluorite-like $[Ln_2O_2]^{2+}$ layers and anti-fluorite-like $[M_2Q_2]^{2-}$ (M = transition metal) layers of edge-linked M$^+$Q$_4$ tetrahedra (e.g., LnCuOQ (Ln = Bi, lanthanide).[29] While most of these materials have been prepared by classical solid-state methods, it is possible to exploit $(Q_2)^{2-}$ dimers in ternary oxy-
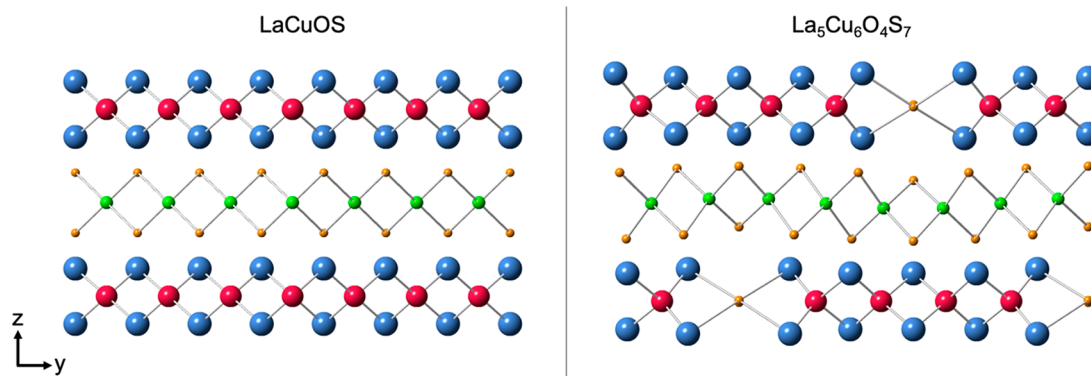
Figure 6. Comparison of LaCuOS and $La_5Cu_6O_4S_7$ crystal structures. Sulfur replaces every fifth oxygen in the $[La_2O_2]^{2+}$ layer. La = blue, O = red, Ch = orange, Cu = green.
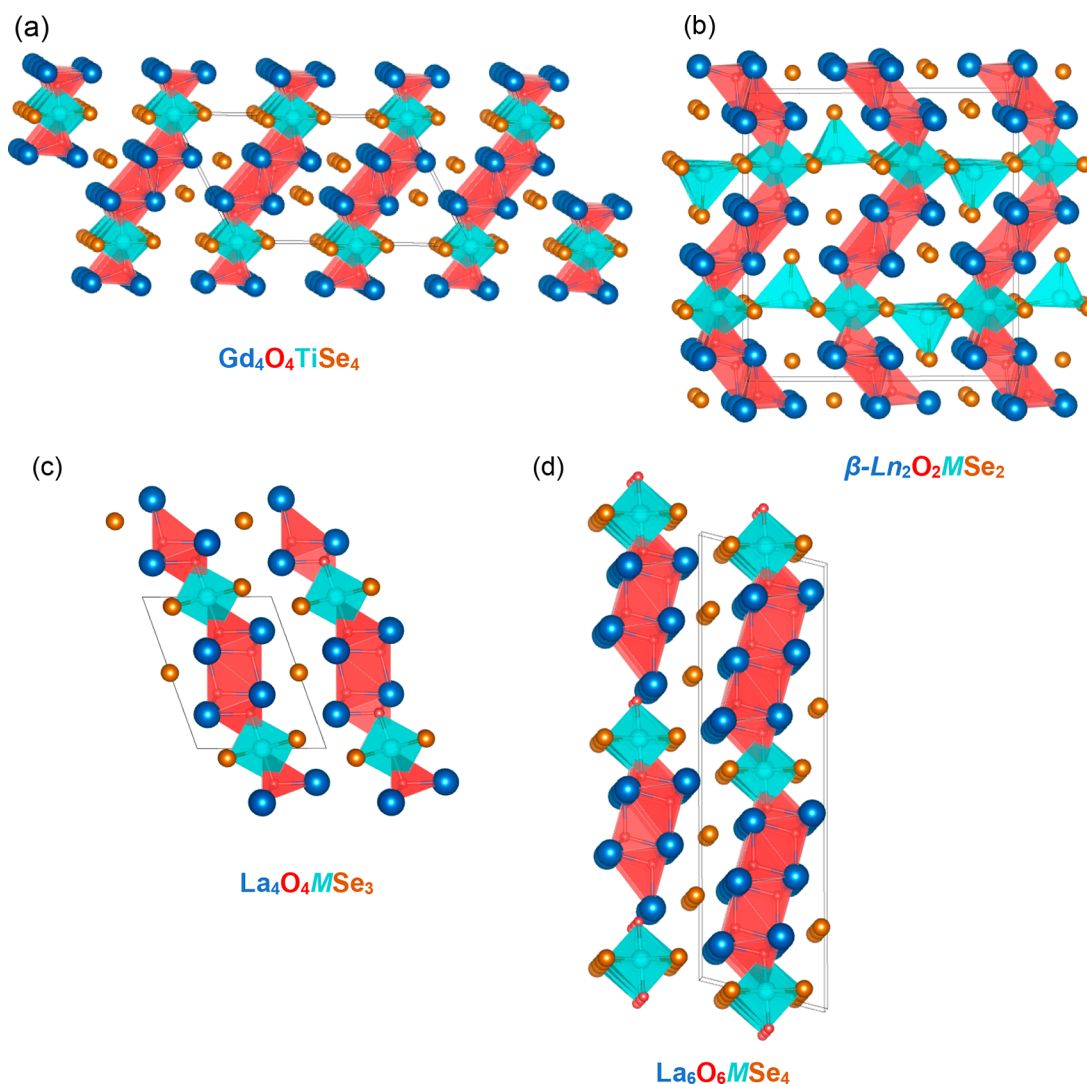
Figure 7. Quaternary Ln−M−O−Q oxychalcogenides with structures containing 2D $[Ln_2O_2]^{2+}$ fragments including (a) $Gd_4O_4TiSe_4$ structure, (b) β-$Ln_2O_2MSe_2$, (c) $La_4O_4MnSe_3$, and (d) $La_6O_6MnSe_4$ with Ln, M, O, and Q ions shown in blue, cyan, pink, and yellow, respectively.

chalcogenides to prepare quaternary materials. If empty σ^* orbitals of $(Q_2)^{2-}$ dimers become occupied, the Q−Q bond can be cleaved by reduction $(Q_2)^{2-} + 2e^- \rightarrow 2Q^{2-}$. Subsequently, vacancies become available for the intercalation of metal atoms.

Upon heating with elemental copper, $La_2O_2S_2$ undergoes a topochemical reaction to achieve LaCuOS.[31] $[La_2O_2]^{2+}$ units remain intact, and the $[La_2O_2]^{2+}$ layers are shifted by $1/2b$. In addition, the S−S bonds within the $(S_2)^{2-}$ dimers undergo rotation and tilt, thereby opening vacant tetrahedral sites. Cu(I) occupies these vacant sites, forming $[Cu_2S_2]^{2-}$ layers
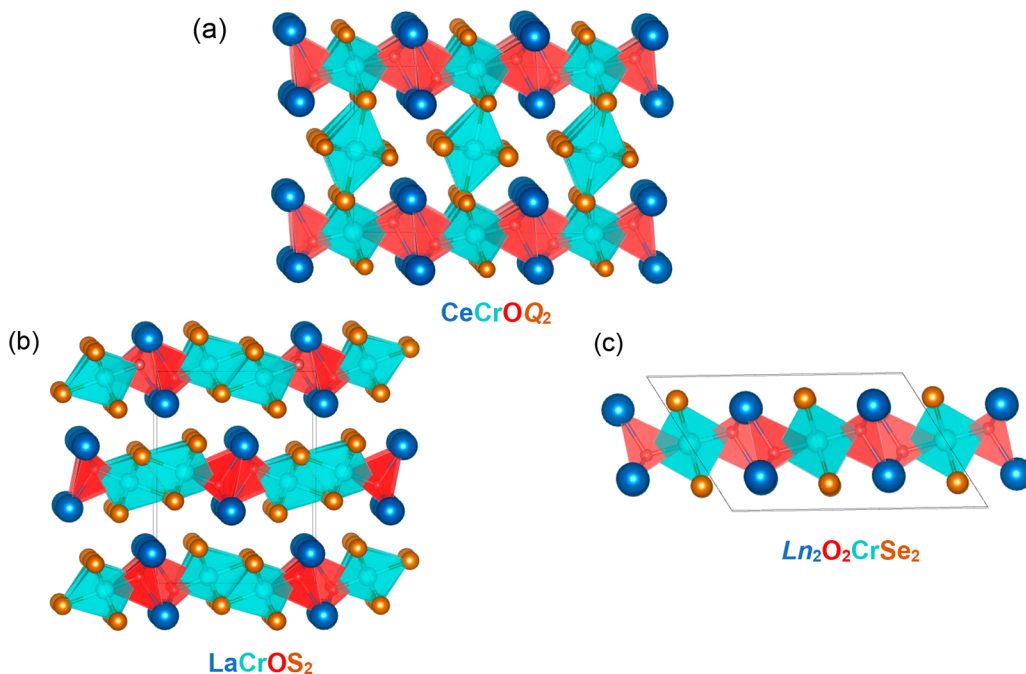
Figure 8. Quaternary Ln−M−O−Q oxychalcogenides with structures containing 1D [LnO]$^+$ ribbons including (a) CeCrOQ$_2$, (b) LaCrOS$_2$, and (c) Ln$_2$O$_2$CrSe$_2$ with Ln, M, O, and Q ions shown in blue, cyan, pink, and yellow, respectively.

reminiscent of Cu−S layers in LaCuOS. The concomitant Cu insertion and breaking of (S$_2$)$^{2-}$ dimers increases the band gap from 2.5 eV for La$_2$O$_2$S$_2$ to 3.1 eV in LaCuOS.[18] An important aspect of this synthetic route is that the topochemical reaction occurs at 340 °C, while heating binary metal oxides, metal sulfides, and Cu together did not successfully yield the quaternary LaCuOS. This further emphasizes the need to exploit bonding of chalcogens to propel materials discovery.

If, on the other hand, classical solid-state synthetic routes (using La$_2$O$_3$, La$_2$S$_3$, Cu, and S) are used, LaCuOS and La$_5$Cu$_6$O$_4$S$_7$ can be achieved. The structure of La$_5$Cu$_6$O$_4$S$_7$ is related to the ZrCuSiAs-type. In La$_5$Cu$_6$O$_4$S$_7$, however, one of every five oxygen atoms in the [010] direction of the [La$_2$O$_2$]$^{2+}$ layer is replaced with a sulfur atom, leading to fluorite-like [La$_5$O$_4$S]$^{2+}$ layers (instead of [La$_2$O$_2$]$^{2+}$).[32] This creates a quasi-1D chain of sulfur (Figure 6). The intriguing consequence here is that the sulfur chains are characterized by split sites, forming (S$_2$)$^{2-}$ dimers. The dimers serve an important role in the material's intrinsic transparency and electrical conductivity.[33]

The LnCuOQ structure is conducive to electronic applications. The insulating [Ln$_2$O$_2$]$^{2+}$ layer can be electronically doped, acting as charge-reservoir layers to the conductivity (or superconductivity) of the intervening chalcogenide layers,[34] and the layered nature of the material can lower the bandwidth of the chalcogenide conduction band.[30] It was recently shown that thin films of NdCuOS containing Cu deficiencies demonstrated an exceptional p-type conductivity (6.4 S·cm^{-1}) and a transparency of ∼50%.[35]

The [Ln$_2$O$_2$]$^{2+}$ layers, often containing fairly heavy cations such as Bi^{3+}, can help reduce the thermal conductivity of these layered materials, enhancing their thermoelectric figure of merit ZT.[34] In the three-anion homologous series, Bi$_{2+2n}$O$_{2+2n}$Cu$_{2-\delta}$Se$_{2+n-\delta}$X$_\delta$ (X = Cl, Br), the increasing number of n Bi$_2$O$_2$Se blocks results in lower band gaps, changes carrier type (from holes to electrons), and reduces thermal

conductivity. Cu vacancies are stabilized by halide substitution of the Se atom.[36,37]

Cation-ordered ZrCuSiAs-related materials are like the ZrCuSiAs-structured materials above. When the M site is occupied by M^{2+}, M sites are half-occupied in an ordered checkerboard (e.g., La$_2$O$_2$CdSe$_2$ in ref 22), stripe fashion (oI polymorphs of Ln$_2$O$_2$MnSe$_2$ and Ln$_2$O$_2$FeSe$_2$ (Ln = La, Ce)[38,39]) or intermediate ordering patterns (Ln$_2$O$_2$MSe$_2$ (Ln = La, Ce; M = Mn, Fe, Zn)[40−42]) (Figure 5c).

Materials that possess a structure like La$_2$O$_2$Fe$_2$OQ$_2$ comprised [Ln$_2$O$_2$]$^{2+}$ layers and [Fe$_2$O]$^{2+}$ layers, separated by Q^{2-} ions. The Fe^{2+} cations are coordinated by both O^{2-} and Q^{2-} anions (forming face-linked FeO$_2$Q$_4$ octahedra), and the presence of O^{2-} in the Fe^{2+} coordination environment contributes to the band narrowing (and Mott insulating nature) of these materials.[43] The magnetic structure of La$_2$O$_2$Fe$_2$OQ$_2$ is stabilized by antiferromagnetic Fe−O−Fe stripes, which are coupled by ferromagnetic Fe−Se−Fe interactions.[44,45] Short-range orthorhombic distortions associated with Fe and O were found in La$_2$O$_2$Fe$_2$OSe$_2$ with neutron pair distribution function analysis. Such short-range distortions may play an important role in Fe-based superconductivity.[46]

2D Fragments in Quaternary Oxychalcogenides. Rather than continuous 2D [Ln$_2$O$_2$]$^{2+}$ layers, discrete 2D [Ln$_2$O$_2$]$^{2+}$ fragments may form, often only three or four OLn$_4$ units long. In contrast to the 2D phases (in which O^{2-} anions only coordinate Ln^{3+} cations), in these fragment phases, the harder O^{2-} anion also forms part of the coordination sphere of the second cation (Figure 7), giving both OLn$_4$ and OLn$_3$M tetrahedra. This might be expected for systems in which the second cation is of intermediate hardness. The Gd$_4$O$_4$TiSe$_4$ family of materials[40,47] illustrates this, with small and highly charged Ti^{4+} cations coordinated by both Se^{2-} and O^{2-} anions forming TiO$_2$Se$_4$ octahedra. The octahedra break up the

$[Gd_2O_2]^{2+}$ units into bands of OGd_4 or OGd_3Ti units (four units wide) that extend along the [010] direction.

$La_4O_4MnSe_3$ is closely related to the $Gd_4O_4TiSe_4$ structure but contains fewer Se^{2-} anions as Ti^{4+} is replaced with Mn^{2+}. For $Gd_4O_4TiSe_4$, the Mn−Se layers are separated by bands of OLa_4 or OLa_3Mn units (four units wide).[25] $La_6O_6MnSe_4$ is an extension of the $La_4O_4MnSe_3$ structure but with wider six-unit wide OLa_4/OLa_3Mn bands separating the Mn−Se layers.[25] In β-$La_2O_2MSe_2$ (oP-$La_2O_2MSe_2$) (M = Mn, Fe)[38,48] two divalent cations (Fe^{2+} or Mn^{2+}) replace Ti^{4+}, forming a tetrahedral MSe_4 site in addition to the octahedral MSe_4O_2 site in the M−Se layers. These M−Se layers are separated by $[La_2O_2]^{2+}$ bands four units wide (as in $Gd_4O_4TiSe_4$). Although the compositions of these phases are the same as the cation-ordered ZrCuSiAs-related phases, their structures are quite different. The polymorphism is influenced by composition and reaction temperature.[38] $La_2O_7VSe_5$ (Figure 4) is composed of V^{3+} cations in VSe_4O_2 octahedra, which break the $[Ln_2O_2]^{2+}$ building units into bands of OLa_4 and OLa_3V units (seven units long) which extend along [100].[25]

Considering the connectivity of the $[Ln_2O_2]^{2+}$ units gave us a way to explore and understand the structural chemistry of the quaternary oxychalcogenides, but often the physical properties of the material rely on the coordination of the M^{x+} cation and the connectivity of its sublattice. Long-range magnetic order results from (often indirect) exchange interactions between magnetic ions, and so the $[Ln_2O_2]^{2+}$ units can influence the magnetic ordering by breaking up magnetic exchange pathways and by separating magnetic layers/chains. Perhaps this is best illustrated by considering β-$La_2O_2MnSe_2$ and the $La_{2n+2}O_{2n+2}MnSe_{n+2}$ series. The $n = 0$ member, β-$La_2O_2MnSe_2$ (Figure 7b), is built from Mn−Se magnetic layers separated by $[Ln_2O_2]^{2+}$ fragments (separation ~8.8 Å) and orders antiferromagnetically below $T_N = 27$ K.[48] The analogous Mn layers in the $n = 1$ member of the series, $La_4O_4MnSe_3$, are separated by ~7 Å, but the Mn cations are separated into pseudo-1D chains (rather than the 2D layers of β-$La_2O_2MnSe_2$).[49] The decreased exchange interactions within the magnetic layers are likely to contribute to the reduced $T_N = 15$ K. With increasing n (i.e., from $n = 0$ mC-$La_2O_2MnSe_2$, $n = 1$ $La_4O_4MnSe_3$, and $n = 2$ $La_6O_6MnSe_4$), the distance between the layers containing the magnetic chains increases. This increased separation might explain the increasingly broad magnetic phase transitions in this series.[25]

1D Ribbons in Quaternary Oxychalcogenides. As the hardness of a second M^{x+} cation in a quaternary oxy-chalcogenide increases, its bonding preferences become more like those of the Ln^{3+} cation. The segregation of O^{2-} and Q^{2-} anions in the structure is reduced, and OLn_4 units are typically less extensive. Several quaternary oxychalcogenides containing +3 cations (e.g., Cr^{3+}, V^{3+}) contain bands of only two OLn_3M units wide, forming one-dimensional "ribbons" that separate M^{x+} cations (Figure 8).

$LnCrOSe_2$ (Ln = Pr, Nd; Q = S, Se)[50] comprises corner-linked chains of edge-shared CrS_6 and edge-sharing CrO_2S_4 octahedra separated by ribbons of two OLn_3Cr tetrahedra. $LnCrOQ_2$ (Ln = Ce−Nd; Q = S, Se) are isostructural to $LaVOSe_2$.[25] (Figure 4).

$Ln_2O_2CrSe_2$ adopts structures closely related to $CeCrOS_2$ but with CrO_2Se_4 chains (instead of CrS_6 octahedra) separated by ribbons of two OLn_3Cr tetrahedra.[51] Hysteretic structural phase transitions are associated with second-order Jahn−Teller distortions of the Cr^{2+} (d^4) ions. Low-temperature neutron diffraction studies show that these materials undergo magnetic transitions associated with both Ln^{3+} and Cr^{2+} ions.

In $La_5V_3O_7Se_6$, edge-sharing VSe_4O_2 octahedra are separated by meandering ribbons of corner and edge-sharing OLa_4 and/or OLa_3V tetrahedra. Two different vanadium sites, V1 and V2, are assigned formal oxidation states of +4 and +3, respectively. In $La_{13}V_7O_{15}Se_{16}$, very curvy ribbons of corner and edge-sharing OLa_4 and/or OLa_3V tetrahedra alternate with ribbons like those seen in $La_5V_3O_7Se_6$ along [010]. The ribbons are linked along [010] at their curves by OLa_3V tetrahedral and VSe_4O_2 octahedral units repeating along [100]. Perpendicular to the ribbons are one-dimensional strands of isolated Se atoms along [100]. $La_{13}V_7O_{15}Se_{16}$ is also mixed valent with V^{3+} and V^{5+} cations. Magnetic ordering of the vanadium moments is observed at low temperatures in these quaternary lanthanum vanadium oxyselenides.[25]

■ A−O−M−Q QUATERNARY OXYCHALCOGENIDES (A = GROUP 1 A⁺ OR GROUP 2 A²⁺ CATIONS)

Whereas the OLn_4 structural unit is ubiquitous in lanthanide quaternary oxychalcogenides, the analogous OA_4 (A = s-block cation) is less common. Cations from groups 1 and 2 are typically softer than Ln^{3+} cations with hardness more comparable to that of M cations.[27] As a result, A and M cations may favor more similar coordination environments, making discrete [AO] units less likely and giving a greater diversity in structural chemistry. This extends the trend described above for Ln−M−O−Q systems with decreasing connectivity of $[Ln_2O_2]^{2+}$ units as the hardness of M cations increases. This preference for the softer chalcogenide anions to play a greater role in A cation coordination as the A cations get softer is illustrated by considering families of quaternary AMOS phases (A = Sr, Ba) (Figure 9).
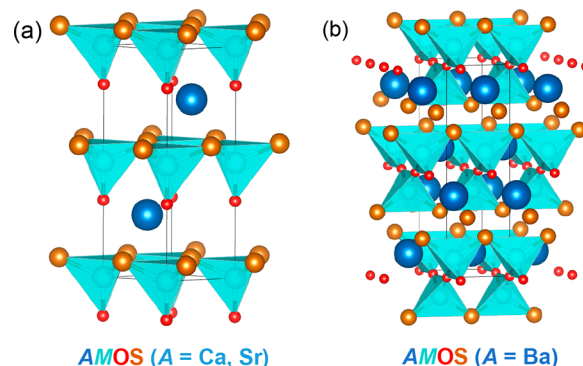
Figure 9. Quaternary A−M−O−Q oxychalcogenides with structures including (a) AMSO (A = Ca, Sr; M = Fe, Co, Zn) and (b) BaMSO (M = Co, Zn) with A, M, O, and Q ions shown in blue, cyan, pink, and yellow, respectively.

SrMOS and CaMOS (M = Fe, Co, Zn)[52−55] form polar structures composed of layers of edge-linked MOS_3 tetrahedra that are coaligned with each other. The A^{2+} cations are coordinated to O^{2-} anions. On the other hand, $BaCoOS$[53] containing larger Ba^{2+} cations (of comparable hardness to the M^{2+} cations) adopt nonpolar structures built up from corner-linked MO_2S_2 tetrahedra which allow the Ba^{2+} cations to be simultaneously coordinated by O^{2-} and S^{2-} anions.

■ SUMMARY

This mini-review presents the structural diversity that has been recently achieved with ternary and quaternary rare-earth oxysulfides and oxyselenides. The OLn_4 tetrahedra are a recurring structural unit in these materials, and variations of these tetrahedra and chalcogen layers diversify structural dimensionality and connectivity. Whether by elemental substitution, modification of dimensionality of OLn_4, OLn_3M, and Q structural motifs, or rearrangement of structural blocks, the crystal structures of oxychalcogenide materials can be tuned to control electrical and magnetic properties. Continued creative synthetic strategies (outside of conventional solid-state synthesis) and high-throughput screening may help to overcome challenges associated with the synthesis of new ternary, quaternary, and even quinary oxychalcogenides[56] for applications in thermoelectrics, transparent conducting materials, and superconductors.

■ ASSOCIATED CONTENT

Ⓢ Supporting Information

The Supporting Information is available free of charge at https://pubs.acs.org/doi/10.1021/acsomega.2c00186.

Tables of quaternary Ln−M−O−S and Ln−M−O−Se compounds, their space groups, unit cell dimensions, and references (XLSX)

■ AUTHOR INFORMATION

Corresponding Author

Robin T. Macaluso − *Department of Chemistry and Biochemistry, University of Texas at Arlington, Arlington, Texas 76019, United States;* ⬥ orcid.org/0000-0002-0021-0775; Email: robin.macaluso@uta.edu

Authors

Melissa Orr − *Department of Chemistry and Biochemistry, University of Texas at Arlington, Arlington, Texas 76019, United States*

Glen R. Hebberd − *Department of Physics, Durham University, Durham DH1 3LE, United Kingdom;* ⬥ orcid.org/0000-0003-4952-9231

Emma E. McCabe − *Department of Physics, Durham University, Durham DH1 3LE, United Kingdom;* ⬥ orcid.org/0000-0001-5868-4570

Complete contact information is available at:
https://pubs.acs.org/10.1021/acsomega.2c00186

Notes

The authors declare no competing financial interest.

Biographies

Melissa S. Orr earned her B.Sc. in Chemistry from the University of Texas at Arlington. In 2020, she received the National Science Foundation Graduate Research Fellowship (NSF-GRFP) and is currently a Ph.D. student working under the supervision of Dr. Robin T. Macaluso. Her research interests are focused on establishing synthetic strategies and structure−property relationships for novel oxytellurides.

Glen R. Hebberd is a first year Ph.D. student at Durham University. Glen's research involves experimental and computational studies into oxysulfide materials for energy applications.

Emma E. McCabe is currently Assistant Professor in Physics at Durham University (U.K.). Emma followed her Ph.D. (University of Birmingham, U.K.) with postdoctoral research at University of Sheffield and Durham University, before being appointed Lecturer and then Senior Lecturer in Chemistry at University of Kent. Her research interests focus on understanding structure−composition− property relationships in functional materials. This includes designing, preparing. and characterizing mixed-anion systems and perovskite-related materials with interesting magnetic, electronic. and dielectric behavior.

Robin T. Macaluso is currently an Associate Professor at the University of Texas at Arlington. She earned her Ph.D. at Louisiana State University and completed postdoctoral studies at Argonne National Laboratory. Her current research interests lie in synthesis of mixed-anion systems and environmental applications of synthetic minerals.

■ REFERENCES

(1) Tripathi, T. S.; Karppinen, M. Mixed-Anion Compounds: An Unexplored Playground for ALD Fabrication. *Adv. Mater. Interfaces* **2021**, *8* (11), 2100146.

(2) Yim, K.; Youn, Y.; Lee, M.; Yoo, D.; Lee, J.; Cho, S. H.; Han, S. Computational Discovery of p-Type Transparent Oxide Semiconductors Using Hydrogen Descriptor. *Npj Comput. Mater.* **2018**, *4* (1), 17.

(3) Zhang, N.; Sun, J.; Gong, H. Transparent p-Type Semiconductors: Copper-Based Oxides and Oxychalcogenides. *Coatings* **2019**, *9* (2), 137.

(4) Tippireddy, S.; D S, P. K.; Das, S.; Mallik, R. C. Oxychalcogenides as Thermoelectric Materials: An Overview. *ACS Appl. Energy Mater.* **2021**, *4* (3), 2022−2040.

(5) Luu, S. D. N.; Vaqueiro, P. Layered Oxychalcogenides: Structural Chemistry and Thermoelectric Properties. *J. Materiomics* **2016**, *2* (2), 131−140.

(6) He, J.; Yao, Z.; Hegde, V. I.; Naghavi, S. S.; Shen, J.; Bushick, K. M.; Wolverton, C. Computational Discovery of Stable Heteroanionic Oxychalcogenides ABXO (A, B = Metals; X = S, Se, and Te) and Their Potential Applications. *Chem. Mater.* **2020**, *32* (19), 8229− 8242.

(7) Kageyama, H.; Hayashi, K.; Maeda, K.; Attfield, J. P.; Hiroi, Z.; Rondinelli, J. M.; Poeppelmeier, K. R. Expanding Frontiers in Materials Chemistry and Physics with Multiple Anions. *Nat. Commun.* **2018**, *9* (1), 772.

(8) Harada, J. K.; Charles, N.; Poeppelmeier, K. R.; Rondinelli, J. M. Heteroanionic Materials by Design: Progress Toward Targeted Properties. *Adv. Mater.* **2019**, *31* (19), 1805295.

(9) Eastman, E. D.; Brewer, L.; Bromley, L. A.; Gilles, P. W.; Lofgren, N. L. Preparation and Properties of the Oxide-Sulfides of Cerium, Zirconium, Thorium and Uranium. *J. Am. Chem. Soc.* **1951**, *73* (8), 3896−3898.

(10) Clarke, S. J.; Adamson, P.; Herkelrath, S. J. C.; Rutt, O. J.; Parker, D. R.; Pitcher, M. J.; Smura, C. F. Structures, Physical Properties, and Chemistry of Layered Oxychalcogenides and Oxypnictides. *Inorg. Chem.* **2008**, *47* (19), 8473−8486.

(11) Carre, D.; Guittard, M.; Jaulmes, S.; Mazurier, A.; Palazzi, M.; Pardo, M. P.; Laruelle, P.; Flahaut, J. Oxysulfides formed by a rare earth and a second metal: II. Shear structures. *J. Solid State Chem.* **1984**, *55* (3), 287−292.

(12) Guittard, M.; Benazeth, S.; Dugué, J.; Jaulmes, S.; Palazzi, M.; Laruelle, P.; Flahaut, J. Oxysulfides and Oxyselenides in Sheets,

Formed by a Rare Earth Element and a Second Metal. *J. Solid State Chem.* **1984**, *51* (2), 227−238.

(13) Figueiredo, M. O. Crystal Chemistry and Layered Structural Description of Oxychalcogenides Involving f-transition Elements. *Inorg. Chim. Acta* **1987**, *140*, 161−164.

(14) Shah, K.; Ćirić, A.; Murthy, K. V. R.; Chakrabarty, B. S. Investigation of a New Way of Synthesis for Nano Crystallites of La$_2$O$_2$S & 1%Ln3+ (Ln = Pr, Eu, Tb, Dy, Er) Doped La$_2$O$_2$S and Study Their Structural and Optical Properties. *J. Alloy. Compd.* **2021**, *851*, 156725.

(15) Strobel, S.; Choudhury, A.; Dorhout, P. K.; Lipp, C.; Schleid, T. Rare-Earth Metal(III) Oxide Selenides M$_4$O$_4$Se[Se$_2$] (M = La, Ce, Pr, Nd, Sm) with Discrete Diselenide Units: Crystal Structures, Magnetic Frustration, and Other Properties. *Inorg. Chem.* **2008**, *47* (11), 4936−4944.

(16) Weber, F. A.; Schleid, T. Über Oxidtelluride (M$_2$O$_2$Te) der leichten Lanthanide (M = La−Nd, Sm−Ho) im A-Typ mit anti-ThCr$_2$Si$_2$-Struktur. *Z. Anorg. Allg. Chem.* **1999**, *625* (11), 1833−1838.

(17) Schmidt, P.; Rademacher, O.; Oppermann, H.; Däbritz, S. II. Zum System Bi$_2$O$_3$/Bi$_2$Se$_3$/Bi$_2$Te$_3$ − die Kristallstruktur von Bi$_2$O$_2$(Te$_x$Se$_{1-x}$). *Z. Anorg. Allg. Chem.* **2000**, *626* (9), 1999−2003.

(18) Koyama, E.; Nakai, I.; Nagashima, K. Crystal chemistry of Oxide-Chalcogenides. II. Synthesis and Crystal Structure of the First Bismuth Oxide-Sulfide, Bi$_2$O$_2$S. *Acta Crystallogr. B* **1984**, *40* (2), 105−109.

(19) Phelan, W. A.; Wallace, D. C.; Arpino, K. E.; Neilson, J. R.; Livi, K. J.; Seabourne, C. R.; Scott, A. J.; McQueen, T. M. Stacking Variants and Superconductivity in the Bi−O−S System. *J. Am. Chem. Soc.* **2013**, *135* (14), 5372−5374.

(20) Larquet, C.; Nguyen, A.-M.; Glais, E.; Paulatto, L.; Sassoye, C.; Selmane, M.; Lecante, P.; Maheu, C.; Geantet, C.; Cardenas, L.; Chanéac, C.; Gauzzi, A.; Sanchez, C.; Carenco, S. Band Gap Engineering from Cation Balance: The Case of Lanthanide Oxysulfide Nanoparticles. *Chem. Mater.* **2019**, *31* (14), 5014−5023.

(21) Graf, C.; Assoud, A.; Mayasree, O.; Kleinke, H. Solid State Polyselenides and Polytellurides: A Large Variety of Se−Se and Te−Te Interactions. *Molecules* **2009**, *14* (9), 3115−3131.

(22) Tuxworth, A. J.; Wang, C.-H.; Evans, J. S. O. Synthesis, Characterisation and Properties of Rare Earth Oxyselenides A$_4$O$_4$Se$_3$ (A = Eu, Gd, Tb, Dy, Ho, Er, Yb and Y). *Dalt. Trans.* **2015**, *44* (7), 3009−3019.

(23) Knop, O.; Boyd, R. J.; Choi, S. C. Sulfur-Sulfur Bond Lengths, or Can a Bond Length be Estimated from a Single Parameter? *J. Am. Chem. Soc.* **1988**, *110* (22), 7299−7301.

(24) Sasaki, S.; Caldes, M. T.; Guillot-Deudon, C.; Braems, I.; Steciuk, G.; Palatinus, L.; Gautron, E.; Frapper, G.; Janod, E.; Corraze, B.; Jobic, S.; Cario, L. Design of Metastable Oxychalcogenide Phases by Topochemical (De)Intercalation of Sulfur in La$_2$O$_2$S$_2$. *Nat. Commun.* **2021**, *12* (1), 3605.

(25) Peschke, S.; Gamperl, L.; Weippert, V.; Johrendt, D. Flux Synthesis, Crystal Structures, and Physical Properties of New Lanthanum Vanadium Oxyselenides. *Dalt. Trans.* **2017**, *46* (19), 6230−6243.

(26) Krivovichev, S. V.; Mentré, O.; Siidra, O. I.; Colmont, M.; Filatov, S. K. Anion-Centered Tetrahedra in Inorganic Compounds. *Chem. Rev.* **2013**, *113* (8), 6459−6535.

(27) Xu, H.; Xu, D. C.; Wang, Y. Natural Indices for the Chemical Hardness/Softness of Metal Cations and Ligands. *ACS Omega* **2017**, *2* (10), 7185−7193.

(28) Mayer, J. M.; Schneemeyer, L. F.; Siegrist, T.; Waszczak, J. V.; Van Dover, B. New Layered Iron-Lanthanum-Oxide-Sulfide and -Selenide Phases: Fe$_2$La$_2$O$_3$E$_2$ (E = S,Se). *Angew. Chem., Int. Ed.* **1992**, *31* (12), 1645−1647.

(29) Johnson, V.; Jeitschko, W. ZrCuSiAs: A "filled" PbFCl type. *J. Solid State Chem.* **1974**, *11* (2), 161−166.

(30) Hiramatsu, H.; Ueda, K.; Kamiya, T.; Ohta, H.; Hirano, M.; Hosono, H. Optical Properties and Two-Dimensional Electronic Structure in Wide-Gap Layered Oxychalcogenide: La$_2$CdO$_2$Se$_2$. *J. Phys. Chem. B* **2004**, *108* (45), 17344−17351.

(31) Sasaki, S.; Steciuk, G.; Guillot-Deudon, C.; Caldes, M. T.; Braems, I.; Janod, E.; Corraze, B.; Jobic, S.; Cario, L. Solvothermal and Mechanochemical Intercalation of Cu into La$_2$O$_2$S$_2$ Enabled by the Redox Reactivity of (S$_2$)$^{2-}$ Pairs. *Dalt. Trans.* **2021**, *50* (36), 12419−12423.

(32) Chan, G. H.; Liu, M.-L.; Chen, L.-D.; Huang, F.-Q.; Bugaris, D. E.; Wells, D. M.; Ireland, J. R.; Hersam, M. C.; Van Duyne, R. P.; Ibers, J. A. Syntheses, Crystal Structures, and Physical Properties of La$_5$Cu$_6$O$_4$S$_7$ and La$_5$Cu$_{6.33}$O4S$_7$. *Inorg. Chem.* **2008**, *47* (10), 4368−4374.

(33) Im, J.; Trimarchi, G.; Poeppelmeier, K.; Zunger, A. Incomplete Peierls-like Chain Dimerization as a Mechanism for Intrinsic Conductivity and Optical Transparency: A La-Cu-O-S Phase with Mixed-Anion Layers as a Case Study. *Phys. Rev. B* **2015**, *92* (23), 235139.

(34) Zhao, L. D.; He, J. Q.; Berardan, D.; Lin, Y. H.; Li, J. F.; Nan, C. W.; Dragoe, N. BiCuSeO oxyselenides: new promising thermoelectric materials. *Energy Environ. Sci.* **2014**, *7* (9), 2900−2924.

(35) Zhang, N.; Liu, X.; Shi, D.; Tang, B.; Annadi, A.; Gong, H. Achievement of Highly Conductive p-Type Transparent NdCuOS Film with Cu Deficiency and Effective Doping. *Mater. Today Chem.* **2018**, *10*, 79−89.

(36) Gibson, Q. D.; Dyer, M. S.; Whitehead, G. F. S.; Alaria, J.; Pitcher, M. J.; Edwards, H. J.; Claridge, J. B.; Zanella, M.; Dawson, K.; Manning, T. D.; Dhanak, V. R.; Rosseinsky, M. J. Bi$_4$O$_4$Cu$_{1.7}$Se$_{2.7}$Cl$_{0.3}$: Intergrowth of BiOCuSe and Bi$_2$O$_2$Se Stabilized by the Addition of a Third Anion. *J. Am. Chem. Soc.* **2017**, *139* (44), 15568−15571.

(37) Gibson, Q. D.; Dyer, M. S.; Robertson, C.; Delacotte, C.; Manning, T. D.; Pitcher, M. J.; Daniels, L. M.; Zanella, M.; Alaria, J.; Claridge, J. B.; Rosseinsky, M. J. Bi$_{2+2n}$O$_{2+2n}$Cu$_{2-\delta}$Se$_{2+n-\delta}$X$_\delta$ (X = Cl, Br): A Three-Anion Homologous Series. *Inorg. Chem.* **2018**, *57* (20), 12489−12500.

(38) Nitsche, F.; Niklaus, R.; Johrendt, D. New Polymorphs of RE$_2$FeSe$_2$O$_2$ (RE = La, Ce). *Z. Anorg. Allg. Chem.* **2014**, *640* (14), 2897−2902.

(39) McCabe, E. E.; Stock, C.; Bettis, J. L.; Whangbo, M. H.; Evans, J. S. O. Magnetism of the Fe^{2+}and Ce^{3+} Sublattices in Ce$_2$O$_2$FeSe$_2$: A Combined Neutron Powder Diffraction, Inelastic Neutron Scattering, and Density Functional Study. *Phys. Rev. B* **2014**, *90* (23), 235115.

(40) Tuxworth, A. J.; Evans, J. S. O. Synthesis, Structure and Properties of the Oxychalcogenide Series A$_4$O$_4$TiSe$_4$ (A = Sm, Gd, Tb, Dy, Ho, Er and Y). *J. Solid State Chem.* **2014**, *210* (1), 188−194.

(41) Ainsworth, C. M.; Wang, C.-H.; Tucker, M. G.; Evans, J. S. O. Synthesis, Structural Characterization, and Physical Properties of the New Transition Metal Oxyselenide Ce$_2$O$_2$ZnSe$_2$. *Inorg. Chem.* **2015**, *54* (4), 1563−1571.

(42) Peschke, S.; Nitsche, F.; Johrendt, D. Flux Synthesis, Modulated Crystal Structures, and Physical Properties of RE-Mn$_{0.5}$SeO (RE = La, Ce). *Z. Anorg. Allg. Chem.* **2015**, *641* (3−4), 529−536.

(43) Zhu, J.-X.; Yu, R.; Wang, H.; Zhao, L. L.; Jones, M. D.; Dai, J.; Abrahams, E.; Morosan, E.; Fang, M.; Si, Q. Band Narrowing and Mott Localization in Iron Oxychalcogenides La$_2$O$_2$Fe$_2$O(Se,S)$_2$. *Phys. Rev. Lett.* **2010**, *104* (21), 216405.

(44) McCabe, E. E.; Stock, C.; Rodriguez, E. E.; Wills, A. S.; Taylor, J. W.; Evans, J. S. O. Weak Spin Interactions in Mott Insulating La$_2$O$_2$Fe$_2$OSe$_2$. *Phys. Rev. B* **2014**, *89* (10), 100402.

(45) Oogarah, R. K.; Suard, E.; McCabe, E. E. Magnetic Order and Phase Transition in the Iron Oxysulfide La$_2$O$_2$Fe$_2$OS$_2$. *J. Magn. Magn. Mater.* **2018**, *446*, 101−107.

(46) Karki, B.; Alfailakawi, A.; Frandsen, B. A.; Everett, M. S.; Neuefeind, J. C.; Xu, B.; Wang, H.; Fang, M.; Freelon, B. Local structure of Mott insulating iron oxychalcogenides La$_2$O$_2$Fe$_2$OM$_2$ (M = Se, Se). *Phys. Rev. B* **2021**, *104* (6), 064101.

(47) Meerschaut, A.; Lafond, A.; Meignen, V.; Deudon, C. Crystal Structure and Magnetic Properties of a New Oxyselenide of Gadolinium and Titanium: Gd$_4$TiSe$_4$O$_4$. *J. Solid State Chem.* **2001**, *162* (2), 182−187.

(48) McCabe, E. E.; Free, D. G.; Mendis, B. G.; Higgins, J. S.; Evans, J. S. O. Preparation, Characterization, and Structural Phase Transitions in a New Family of Semiconducting Transition Metal Oxychalcogenides β-La$_2$O$_2$MSe$_2$ (M = Mn, Fe). *Chem. Mater.* **2010**, *22* (22), 6171−6182.

(49) Peschke, S.; Johrendt, D. Flux Synthesis, Crystal Structures, and Magnetism of the Series La$_{2n+2}$MnSe$_{n+2}$O$_{2n+2}$ (n = 0−2). *Inorganics* **2017**, *5* (1), 9.

(50) Zhang, X.; Xiao, Y.; Wang, R.; He, J.; Wang, D.; Bu, K.; Mu, G.; Huang, F. Synthesis, Crystal Structure, and Physical Properties of Layered LnCrSe$_2$O (Ln = Ce−Nd). *Inorg. Chem.* **2019**, *58* (14), 9482−9489.

(51) Peschke, S.; Weippert, V.; Senyshyn, A.; Mühlbauer, M. J.; Janka, O.; Pöttgen, R.; Holenstein, S.; Luetkens, H.; Johrendt, D. Flux Synthesis, Crystal Structures, and Magnetic Ordering of the Rare-Earth Chromium(II) Oxyselenides RE$_2$CrSe$_2$O$_2$ (RE = La−Nd). *Inorg. Chem.* **2017**, *56* (4), 2241−2247.
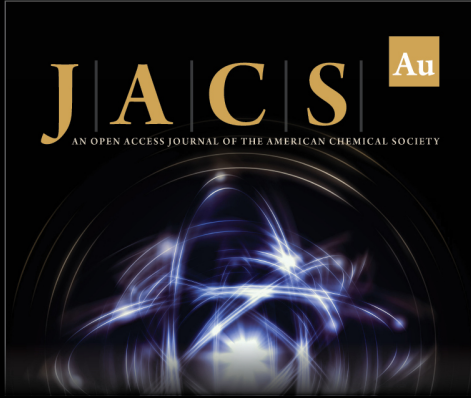
(52) Liu, W.; Lai, K. T.; Eckhardt, K.; Prots, Y.; Burkhardt, U.; Valldor, M. Synthesis and Characterization of Sulfide Oxide SrZnSO with a Strongly Polar Crystal Structure. *J. Solid State Chem.* **2017**, *246*, 225−229.

(53) Salter, E. J. T.; Blandy, J. N.; Clarke, S. J. Crystal and Magnetic Structures of the Oxide Sulfides CaCoSO and BaCoSO. *Inorg. Chem.* **2016**, *55* (4), 1697−1701.

(54) Jin, S. F.; Huang, Q.; Lin, Z. P.; Li, Z. L.; Wu, X. Z.; Ying, T. P.; Wang, G.; Chen, X. L. Two-Dimensional Magnetic Correlations and Partial Long-Range Order in Geometrically Frustrated CaOFeS with Triangle Lattice of Fe Ions. *Phys. Rev. B* **2015**, *91* (9), 094420.

(55) Delacotte, C.; Pérez, O.; Pautrat, A.; Berthebaud, D.; Hébert, S.; Suard, E.; Pelloquin, D.; Maignan, A. Magnetodielectric Effect in Crystals of the Noncentrosymmetric CaOFeS at Low Temperature. *Inorg. Chem.* **2015**, *54* (13), 6560−6565.

(56) Williamson, B. A. D.; Limburn, G. J.; Watson, G. W.; Hyett, G.; Scanlon, D. O. Computationally Driven Discovery of Layered Quinary Oxychalcogenides: Potential p-Type Transparent Conductors? *Matter* **2020**, *3* (3), 759−781.